*Korean J. Chem. Eng.*, 37(4), 614-622 (2020)
DOI: 10.1007/s11814-020-0484-7

pISSN: 0256-1115
eISSN: 1975-7220

# Silver and palladium nanoparticle embedded poly(n-isopropylacrylamide-*co*-2-acrylamido-2-methylpropane sulfonic acid) hybrid microgel catalyst with pH and temperature dependent catalytic activity

**Abdul Haleem*, Sidra Bibi Syaal**, Muhammad Ajmal***, Jaweria Ambreen****, Sajid Rauf*****, Nasir Ali******, Saz Muhammad**, Afzal Shah**,*******, Muhammad Abid Zia***, and Muhammad Siddiq*,***,†**

*CAS Key Laboratory of Soft Matter Chemistry, Department of Polymer Science and Engineering, University of Science and Technology of China, Hefei, Anhui 230026, China
**Department of Chemistry, Quaid-i-Azam University, Islamabad 45320, Pakistan
***Department of Chemistry, University of Education, Attock Campus, Attock 43600, Pakistan
****Department of Chemistry, COMSATS University Islamabad, Parkroad, 45550, Islamabad, Pakistan
*****Hubei Collaborative Innovation Center for Advanced Organic Chemical Materials, Faculty of Physics and Electronic Science, Hubei University, Wuhan, Hubei 430062, P. R. China
******Zhejiang Province Key Laboratory of Quantum Technology and Devices and Department of Physics, State Key Laboratory for Silicon Materials, Zhejiang University, Hangzhou, 310027, P. R. China
*******Department of Chemistry, College of Science University of Bahrain, Sakhir 32038, Bahrain
(*Received 11 September 2019 • accepted 5 January 2020*)

**Abstract**−Here in, we demonstrate facile fabrication of silver and palladium nanoparticles in dual responsive poly(N-isopropylacrylamide-*co*-2-Acrylamido-2-methylpropane sulfonic acid) microgel with temperature- and pH-dependent catalytic potential. Palladium-based catalyst showed better catalytic efficiency as compared to silver-based catalyst for degradation of Rhodamine-B and P-Nitrophenol in aqueous medium under the same set of reaction conditions. The responsive nature of the microgel was found to be useful to tune the catalytic activity of the as-prepared catalysts, and reduction rate was enhanced with the pH and temperature elevation of the reaction medium; however, the increasing trend was slowed in the volume phase transition region of the microgel. Under a specific set of reaction conditions, the reduction of Rhodamine-B was as fast as 0.968 and 0.571 $min^{-1}$ when catalyzed with palladium and silver based catalysts, respectively. The hydrodynamic radius of the particles of microgel support was found to be in the range of 65-180 nm when pH and temperature of the medium were varied in the range of 2-12 and 25-45, respectively. The estimated diameter of silver and palladium nanoparticles fabricated in the microgel support under the same set of reaction conditions was 9-15 and 7-11 nm, respectively.

Keywords: Microgel, Nanoparticle, Catalysis, P-nitrophenol, Rhodamine-B

## INTRODUCTION

Most textile industries are releasing toxic dyes and organic pollutants that cause water pollution, which needs amelioration and prevention. Human beings, as well as aquatic organisms, are seriously affected by these organic pollutants like dyes and nitro compounds [1-4]. They have worst effects on human eyes, skin, and respiratory system. For the elimination of these harmful organic pollutants, different techniques such as flocculation, physical adsorption, chemical degradation, and photo degradation have been utilized. Many strategies have been employed to degrade these harmful organic pollutants to harmless products [5-7]. Metallic catalysts like gold and silver belonging to transition metals have been used for degrading dyes, organic aromatic compounds, as well as microorganisms. Mostly, metals act as catalysts when they are in nanosized domain. Generally, the catalytic potential is supposed to originate from their high surface to volume ratio, which varies with particle size. Therefore, the catalytic potential has been found to depend on particle size of catalyst and varies directly with particle size. However, for very small catalysts (diameter ≤1), which are named as cluster of atoms instead of nanoparticles, the catalytic potential depends on enumeration of special sites, i.e., atoms present at the corner and edges of the cluster. At such a small scale, direct relationship of particle size and catalytic potential is not operative. For example, a catalytic study on a range of platinum (Pt) clusters supported on magnesia composed of $Pt_n$ (n=8-15) atoms has revealed that maximum activity was observed with a cluster of $Pt_{13}$ [8]. The researchers also showed that catalysts with enhanced selectivity along with reasonable catalytic potential, under specific conditions for specific reactions, can be designed in the form of supported single atoms [9]. While investigating the catalytic performance of catalysts composed of single atom of Pt to its nanoparticles with diameter of 2 nm, it was observed that in subnanometer regime the selectivity was enhanced but activity was suppressed in the semi-

†To whom correspondence should be addressed.
E-mail: m_sidiq12@yahoo.com

hydrogenation of acetylene to ethylene [10]. The studies show that the exact relation between activity and selectivity of catalysts at subnanometer regime is still debatable. On the other hand, metal nanoparticles are supposed to perform catalytic action that stems from their high surface to volume ratio. Owing to their high surface area and weak intermolecular forces, metal nanoparticles (MNPs) tend to aggregate in the aqueous phase that decreases their catalytic activity. To avoid the agglomeration of MNPs, hydrogels, metal oxide supports, mesoporous and microporous materials are used. Hydrogels are becoming the more focused carrier among all other types of the carrier systems since they absorb huge amount of water, therefore providing exceptional medium for the aqueous catalytic reaction [11-14]. In addition they also enable the recycling of nanocatalysts without any loss or leaching of catalyst by an easy, quick and economical process of filtration or centrifugation depending upon the condition of hydrogel network. Hydrogel networks contain metal binding sites such as -COOH, OH, -SH, $NH_2$, $-SO_3H$ that facilitate the uptake of high amount of metallic ions from aqueous media. A suitable reducing agent could do in-situ reduction of the metallic ions which could transform into nanoparticles and get arranged into the hydrogel matrices because of electrostatic and ion-dipole attractions. Additionally, the ability to sense the physical or chemical changes in environment makes these hydrogels stimuli-responsive and usable in a variety of applications [15]. Among various types of hydrogels, microgels show rapid response to the environment owing to their small dimensions as compared to macro or bulk hydrogels. Poly(N-isopropylacrylamide) has formally been used to stabilize nanoparticles and become popular among other stimuli-responsive polymers [16-19]. Additionaly, p(Nipam) microgel network can also be fabricated in the presence of cross-linker via polymerization method. Moreover, colloidally stable multiple responsive pNipam micro or nanoparticles can also be synthesized via copolymerization with other functional monomers [20,21]. Han et al. used p(Nipam-co-acrylic acid) microgel as a matrix for the in-situ generation of Ag nanoparticle for $H_2O_2$ sensing [22]. Similarly, Liu et al. introduced Ag-nanoparticle into the p(Nipam) microgel to study the temperature-dependent catalytic activity [23]. It was observed that by changing the temperature, the catalytic ability of hybrid microgel can be controlled easily. Likewise, Sahiner et al. used a different molar ratio of poly(acrylamide-co-vinylsulphonic acid) hydrogels as a matrix for nickel and cobalt nanoparticles and used this hybrid microgel to catalyze the production of hydrogen by the hydrolysis of $NaBH_4$ [24]. Shah et al. loaded Ag-nanoparticles to cationic poly (N-isopropylacrylamide-vinylaceticacid-acrylamide) microgel and utilized it for reducing P-Nitrophenol (P-NP) to P-Aminophenol (P-AP) [25]. The hybrid microgel was found to be stable in the pH range of 3.0-9.3. Zhang et al. observed the optical properties of multifunctional microgel as a function of temperature, pH, and UV-Visible irradiation [26]. A red shift was observed in the reflectance peaks of etalons by changing the microgels from swollen to collapsed form. Ajmal et al. investigated the multi-responsive hybrid microgels for the stabilization of silver NPs as a catalyst for the reduction of P-NP to P-AP [27].

Here in, a dual pH and temperature, sensitive p(Nipam-Amps) microgel has been synthesized via emulsion polymerization. Further, silver (Ag) and palladium (Pd) metal nanoparticles were fabricated in the microgel by in situ reduction method to form Ag- and Pd-p(Nipam-Amps) hybrid microgels, respectively. The presence of Ag and Pd nanoparticles in p(Nipam-Amps) microgel induced optical and catalytic characteristics in the resultant Ag- and Pd-p(Nipam-Amps) hybrid microgels. The catalytic performance was observed in degrading the Rhodamine-B (RhB) and P-NP using water as reaction medium.

## MATERIALS AND METHODS

N-isopropyl acrylamide (Nipam, 99% purity, J&K Chemical), acrylamide-2-methyl-1-propanesulfonic acid (Amps, 99% purity, J&K Chemical), N,N-methylene bisacrylamide (MBA, 99% purity, Sinopharm Chemical Reagents Co.), sodium dodecylsulphate (SDS, 99% purity, Aladdin), ammonium persulfate (APS, 99% purity, Aladdin), silver nitrate ($AgNO_3$, 99% purity, Aladdin), palladium chloride ($PdCl_2$, 99% purity, Aladdin), sodium borohydride ($NaBH_4$, Sinopharm Chemical Reagents Co.), sodium hydroxide (NaOH, Sinopharm Chemical Reagents Co.), hydrochloric acid (HCl, Sinopharm Chemical Reagents Co.) were used as received. Nipam and Amps were purified before use for good polymerization yield. Nipam was purified by recrystallization method by dissolving 30 g of Nipam in 20 mL of benzene at 45 °C while, Amps was purified by recrystallization method by dissolving 20 g of it in 50 mL of methanol at 50 °C.

### 1. Synthesis of Pure p(Nipam-Amps) Microgel

P(Nipam-Amps) microgel was synthesized by aqueous emulsion polymerization. Shortly, in a 100 ml three-necked round bottom flask containing 95 ml deionized water we added 1.222 g Nipam, 0.1243 g Amps, 0.0925 g MBA and 0.05 g SDS before fortifying with temperature controlled oil bath, condenser and nitrogen inlet. In the next step, stirring was done at the rate of 500 rpm under continuous nitrogen purging and by maintaining the temperature at 70 °C±2 °C. The polymerization process was activated with the injection of APS (0.055 g dissolved in 5 ml of water) in the reaction flask. The reaction was allowed to proceed at the set constant under a continuous supply of $N_2$ gas for 5 hrs. Milky appearance in the first 30 mins indicated that the reaction had started. Stirring and heating were stopped after five hours. The reaction mixture was cooled to room temperature. Subsequently, the prepared gel was transferred to a dialysis membrane and suspended in deionized water for four days. On the first day, water was changed three times. For the next three days water was changed two times each day. The microgel was removed from dialysis membrane and centrifuged at 20,000 rpm for 5 mins.

### 2. Fabrication of Silver and Palladium Based Hybrid Microgel Catalysts

For the fabrication of Ag-p(Nipam-Amps) hybrid microgel, 10 ml of pure microgel was diluted in a three-necked round bottom flask by 30 ml water and stirred under nitrogen purging to remove the dissolved oxygen from the reaction medium. After 30 mins, 10 ml of 3 mM of silver salt was added under continuous stirring and nitrogen atmosphere. In the next step, after an hour, a fresh solution of $NaBH_4$ (0.03 g in 5 ml deionized water) was injected into the solution dropwise and the reaction was continued for two hours. Immediately, when $NaBH_4$ was added, a dark brown color appeared as shown in Fig. 1(a), confirming the formation of Ag nanoparti-

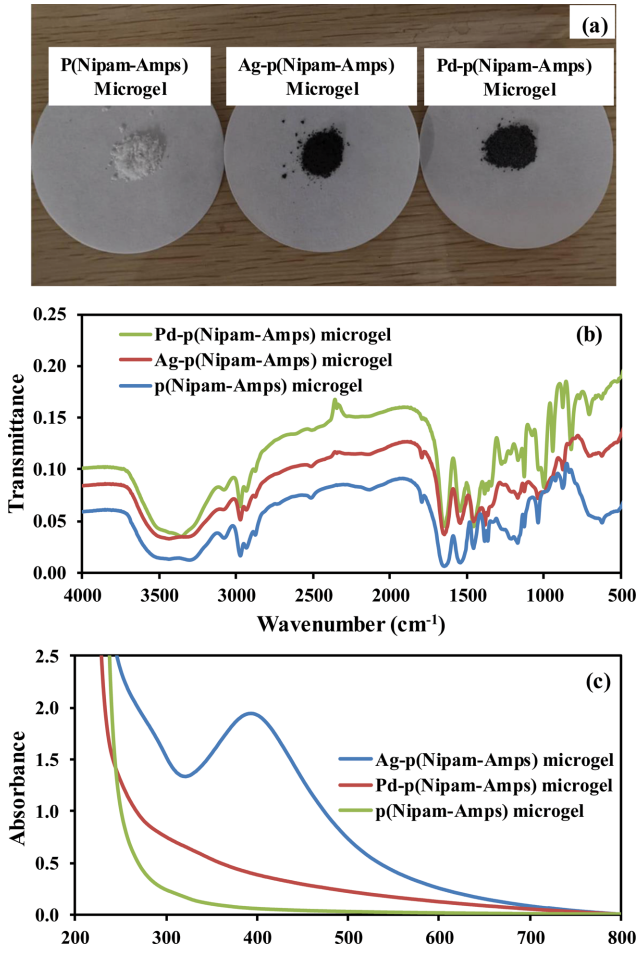


**Fig. 1. (a) Photographs of the p(Nipam-Amps) microgel, Ag-p(Nipam-Amps) hybrid microgel and Pd-p(Nipam-Amps) hybrid microgel. (b) FT-IR spectra of p(Nipam-Amps) microgel, Ag-p(Nipam-Amps) hybrid microgel and Pd-p(Nipam-Amps) hybrid microgel. (c) UV-Vis spectra of of p(Nipam-Amps) hybrid microgel, Ag-p(Nipam-Amps) hybrid microgel and Pd-p(Nipam-Amps) microgel.**

cles. After two hours, the stirring and $N_2$ purging was stopped and the obtained Ag-p(Nipam-Amps) hybrid microgel was purified through dialysis membrane for hour hours, while changing the water after each hour. Afterwards, the composite was freeze dried and stored for further characterizations and applications. A similar procedure was used for Pd-p(Nipam-Amps) hybrid microgel where the color of the system turned light black as depicted in Fig. 1, indicating the fabrication of Pd nanoparticles in p(Nipam-Amps) hybrid microgel.

### 3. Catalytic Experiments

20 ml of 0.016 mM aqueous solution of rhodamine B was taken as our target reactant to be reduced. 0.02 g of $NaBH_4$ was added as a reducing agent. The pH of the reaction medium was adjusted by the addition of concentrated aqueous solution of NaOH or HCl. The temperature of the reaction medium was maintained using a temperature controlled oil bath. The catalytic reduction was carried out by using 20-60 μL of the as-prepared Pd- or Ag-p(Nipam-Amps) hybrid microgel as a catalyst. After specific intervals of time, absorbance of the reaction mixture was recorded with UV-Vis spectrophotometer. In case of P-Nitrophenol, 20 ml of 0.05 mM aqueous solution was taken as our target reactant to be reduced. The rest of the process was quite similar to that adopted for Rhodamine-B.

### 4. Characterization Techniques

For functional group analysis, Fourier-transform infrared (FTIR) spectroscopy was performed on a Bruker VECTOR-22 IR spectrometer using KBr discs. The colloidal particle size in terms of average hydrodynamic diameter was measured on a zetasizer (Malvern Zetasizer Nanoseries). Crystalline nature, thermal behavior, elemental analysis, and nanoparticles distribution were analyzed by X-ray powder diffraction (XRD, Smart Lab, Rigaku), Thermal gravimetric analysis (TGA, PE TGA-7), Energy-dispersive X-ray spectroscopy (EDS) and Transmission electron microscopy (TEM, Hitachi H-7650, 100 kV). UV-Visible spectroscopy (Shimadzu, UV-3600) was used for catalytic activity.

## RESULTS AND DISCUSSION

The successful copolymerization of Nipam and Amps was confirmed by FT-IR analysis, carried out in the range of 500-4,000 $cm^{-1}$. Fig. 1(b) shows the FTIR spectra for p(Nipam-Amps) hybrid microgel, Ag-p(Nipam-Amps) hybrid microgel and Pd-p(Nipam-Amps) hybrid microgel. Polymerization was confirmed by the disappearance of characteristic bands at 3,000-3,100 $cm^{-1}$, which corresponds to -CH of olefin. The broad peaks around 1,647 $cm^{-1}$ and 1,040 $cm^{-1}$ can be attributed to the amide group of carbonyl functionality and sulfonic group, respectively. Moreover, peaks around 2,973, 1,550, 1,461, and 1,381 $cm^{-1}$ can be assigned to the O-H stretching [28], -N-H vibration [29], -C-H bending of $-CH_2$ groups [30] and isopropyl group vibration [31], present in pure and hybrid microgels. There is no noticeable difference in positions of absorption bands of all three samples, which confirms that the hydrogel network retained its identity after the incorporation of metal nanoparticles. To further confirm the existence of nanoparticles, UV-Visible spectroscopic analysis was carried out. From Fig. 1(c), it is quite obvious that AgNPS are present in polymer network with a typical plasmonic peak around 400 nm, while in the case of Pd-p(Nipam-Amps) hybrid microgel, there is no such peak observed in the same range, which is due to absence of plasmonic characteristics in PdNPS; these observations are in line with the reported literature [32]. The particle size distribution of fabricated dual sensitive microgel was also carried out through zetasizer to study their responsive behavior.

A microgel system is pH sensitive due to the existence of Amps moiety while thermosensitivity comes because of Nipam moieties present in the polymer network. In the first step, we studied the effect of pH (2-10) on the hydrodynamic radius at room temperature. Fig. 2(a) represents the results of effect of pH on particle size of p(Nipam-Amps) microgel.

At low pH, the particle size was very small, in the range of 80 nm. With an increase in pH, the hydrodynamic diameter increased and particle size reached to 190 nm. Such an increase in hydrodynamic diameter was observed due to repulsion between negative charges on polymeric network which are produced to the deprotonation of sulfonic groups at higher pH (basic medium) [33]. The

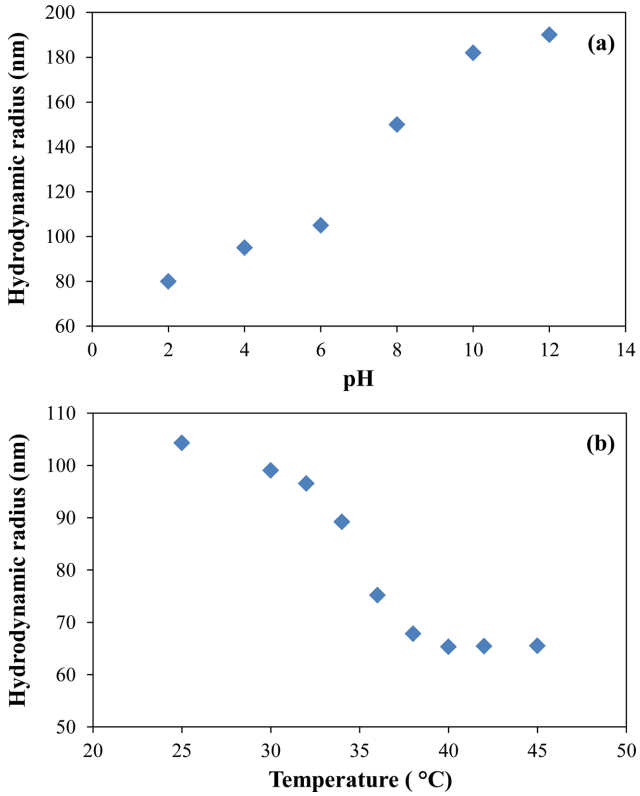


**Fig. 2. Volume phase transition in p(Nipam-Amps) microgel particles in terms of variation in hydrodynamic radius as a function of (a) pH and (b) temperature.**

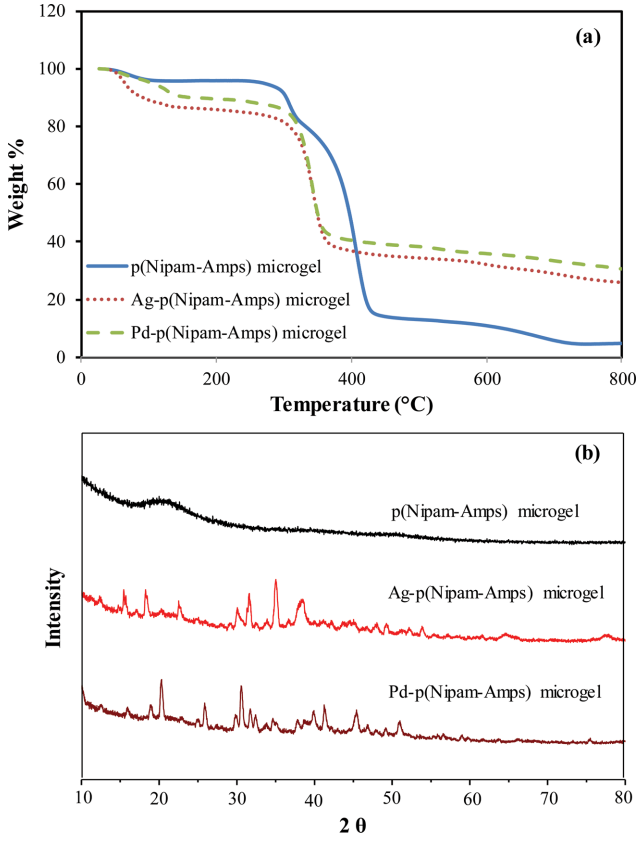


**Fig. 3. (a) TGA thermograms of p(Nipam-Amps) microgel, Ag-p(Nipam-Amps) hybrid microgel and Pd-p(Nipam-Amps) hybrid microgel. (b) XRD patterns of p(Nipam-Amps) microgel, Ag-p(Nipam-Amps) hybrid microgel and Pd-p(Nipam-Amps) hybrid microgel.**

negatively charged sulfonic groups execute repulsion among the polymer chains in p(Nipam-Amps) microgel network resulting in swelling of the network and hence increasing the particle size at higher pH of the medium. We also studied the effect of temperature (25-45 °C) on hydrodynamic radius of microgel with DLS by keeping the pH of the medium around 6.5 (pH of the as-prepared microgel) as shown in Fig. 2(b). At low temperature, the hydrodynamic diameter is large and the particle size comes in the range of 105 nm. The large amount of water present in the polymer network is the main reason for the large particle size. It indicates that at low temperature it behaves like a hydrophilic material, which is obvious due to dominant hydrophilic characteristics of Nipam moieties. By increasing the temperature the particle size is decreased. It is due to effective hydrophobic characteristics of Nipam at its lower critical solution temperature (LCST) of 32 °C. With an increase in temperature from 25 °C to 32 °C, no pronounced effect occurred on the particle size; however, on further increase in temperature from 32 °C to 38 °C the hydrodynamic radius of p(Nipam-Amps) microgel particles shrank prominently to 65 nm. This shrinkage is due to hydrophobic characteristics of Nipam moiety, which brings the polymer chains close to each other and expels the water out of the polymer network. Further increase in the temperature from 38 °C to 45 °C did not affect the particle size, which confirms that microgel was shrunk to its maximum capacity at 38 °C. Thermal stability of the bare, Ag-p(Nipam-Amps) and and Pd-p(Nipam-Amps) hybrid microgel was examined by TGA in the range of 100-800 °C as shown in the Fig. 3(a). The p(Nipam-Amps) microgel showed thermal decomposition in four steps. Initially, the degradation started from 50 °C and ended at 95 °C with 4% weight loss, that can be attributed to the dehydration of the polymer matrix. In the second step almost 12% of the sample mass was degraded in the range of 260-320 °C, which can be attributed to the thermal breakdown of loosely held polymer chains at the surface of microgel network. Further degradation occurred in the range of 320-430 °C where of 85% of the sample weight was degraded. This weight loss can be assigned to the breakage of the polymer backbone chain. Finally, almost 97% of the sample was degraded in the range of 430-800 °C, confirming the complete decomposition of the polymer network. The non-volatile residues at 800 °C were only 3%. While in the case of Ag- and Pd-p(Nipam-Amps) hybrid microgel showed three-step thermal degradation. In case of Pd-p(Nipam-Amps) hybrid microgel, first thermal decomposition occurred in the temperature range of 50-160 °C with 10% weight loss, while second and third decomposition occurred in the range of 230-365 °C and 365-800 °C where total weight loss increased to 60% and 70%, respectively.

Similarly, in case of Ag-p(Nipam-Amps) hybrid microgel the degradation occurred in three steps, but the final weight loss was 75%, which confirms that Pd-p(Nipam-Amps) hybrid microgel is thermally more stable as compared to Ag-p(Nipam-Amps) hybrid

microgel and p(Nipam-Amps) microgel. Increase in residual weight was observed due to the presence of Pd and Ag nanoparticles in the matrix of p(Nipam-Amps) microgel. Amorphous and crystalline nature of bare and hybrid microgel was analyzed from their XRD patterns, shown in Fig. 3(b). In the case of p(Nipam-Amps) microgel, a broad peak was observed around 15-25°, confirming the amorphous nature of p(Nipam-Amps) microgel. While in the case of Pd- and Ag-p(Nipam-Amps) hybrid microgels sharp peaks were observed, confirming the crystalline nature of the fabricated Pd- and Ag-p(Nipam-Amps) hybrid microgels. All the reflections were indexed as (111), (200), (220) and (311) with corresponding 2 theta values with 38.48°, 44.44°, and 64.54° and 77° representing Ag nanoparticles with face-centered cubic (Fcc) symmetry [34]. The peaks around 20° to 30° correspond to pure microgel. Similarly, all the reflections indexed as a (111), (200) and (220) with corresponding 2 theta values of 39.93°, 45.42° and 67.40° confirmed the presence of Pd nanoparticles in microgel network [32,35,36]. Elemental analysis was carried out by EDX to ensure the presence of Ag and Pd content in the p(Nipam-Amps) microgel. It was observed that 5.14 wt% of Ag-p(Nipam-Amps) hybrid microgel was comprised of Ag, while 1.62 wt% of Pd-p(Nipam-Amps) hybrid microgel was composed of Pd. The EDX spectra of Pd-p(Nipam-Amps) hybrid microgel and Ag-p(Nipam-Amps) hybrid microgel are shown Fig. 4(a) and (b), respectively. The results demonstrate that the amount of Ag absorbed per unit mass of p(Nipam-Amps) microgel was greater than that of Pd. Since the functional groups of p(Nipam-Amps) microgel are responsible for the absorption of metal ions, this difference can be attributed to different affinity of functional groups of p(Nipam-Amps) microgel for the Ag and Pd. The results of EDX also suggest that number of Pd ions in each mesh of p(Nipam-Amps) microgel would be lower than that of Ag.

For particle size analysis, we used transmission electron microscopy (TEM). The TEM images are shown in Fig. 5. In the case of Ag-p(Nipam-Amps) hybrid microgels, the diameter of Ag NPS ranges from 9-15 nm as shown in Fig. 5(a). While in the case of Pd-p(Nipam-Amps) hybrid microgels, the diameter of Pd nanoparticles is smaller as compared to Ag NPs. The size of Pd NPs was calculated to be in the range of 7-11 nm, as shown in Fig. 5(b).

The smaller particle size of Pd agrees with EDX results, which demonstrates that the number of Pd ions in each mesh of p(Nipam-Amps) microgel was lower than that of Ag. The collection of metal ions in a mesh acts as precursor of corresponding metal nanoparticles, and lower number of precursors result in the formation of smaller nanoparticles. Moreover, TEM images confirmed that the prepared nanoparticles were highly stable inside the polymer network without a noticeable aggregation.

**1. Degradation of Rhodamine B**

The catalytic activity of synthesized Pd- and Ag-p(Nipam-Amps) hybrid microgels was tested for the degradation of Rhodamine B. Since, Rhodamine B is a toxic dye and discharges directly from the textile industry into water drains. Hence, its degradation or elimination is very vital. Therefore, catalytic degradation of Rhodamine B was chosen as model reaction to attest to the catalytic potential of the prepared catalysts. The effect of pH, temperature and concentration of catalysts on the degradation rate of Rhodamine B was studied. The degradation was observed by using UV-visible spectroscopy, as Rhodamine B gives a prominent absorption peak in the visible region at 554 nm. The effect of our catalyst on Rhodamine

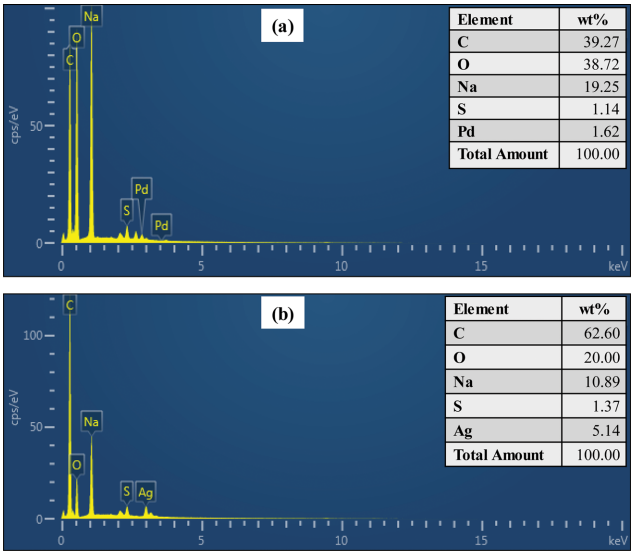


**Fig. 4. EDX spectra of (a) Pd-p(Nipam-Amps) hybrid microgel and (b) Ag-p(Nipam-Amps) hybrid microgel.**

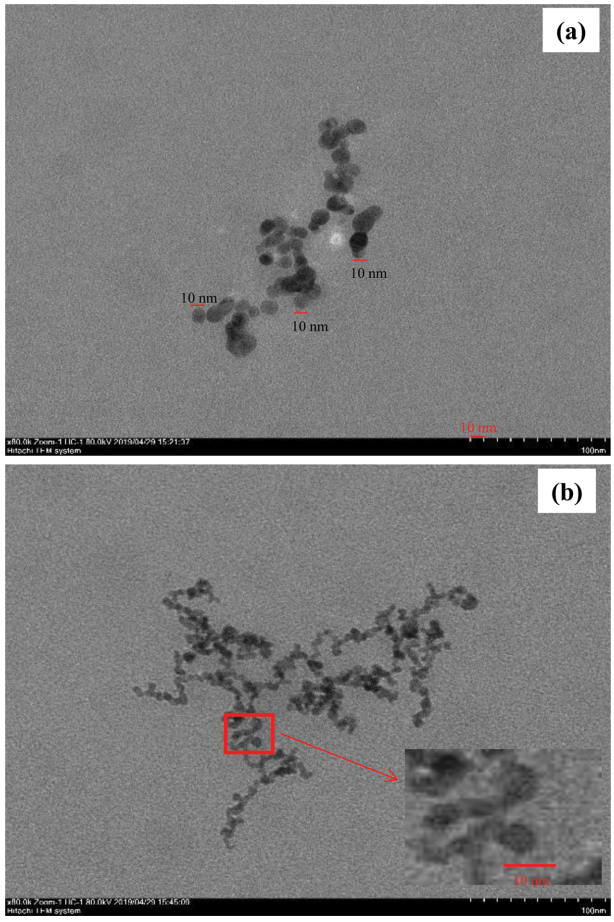


**Fig. 5. TEM image of (a) Ag and (b) Pd nanoparticles embedded in p(Nipam-Amps) microgel.**

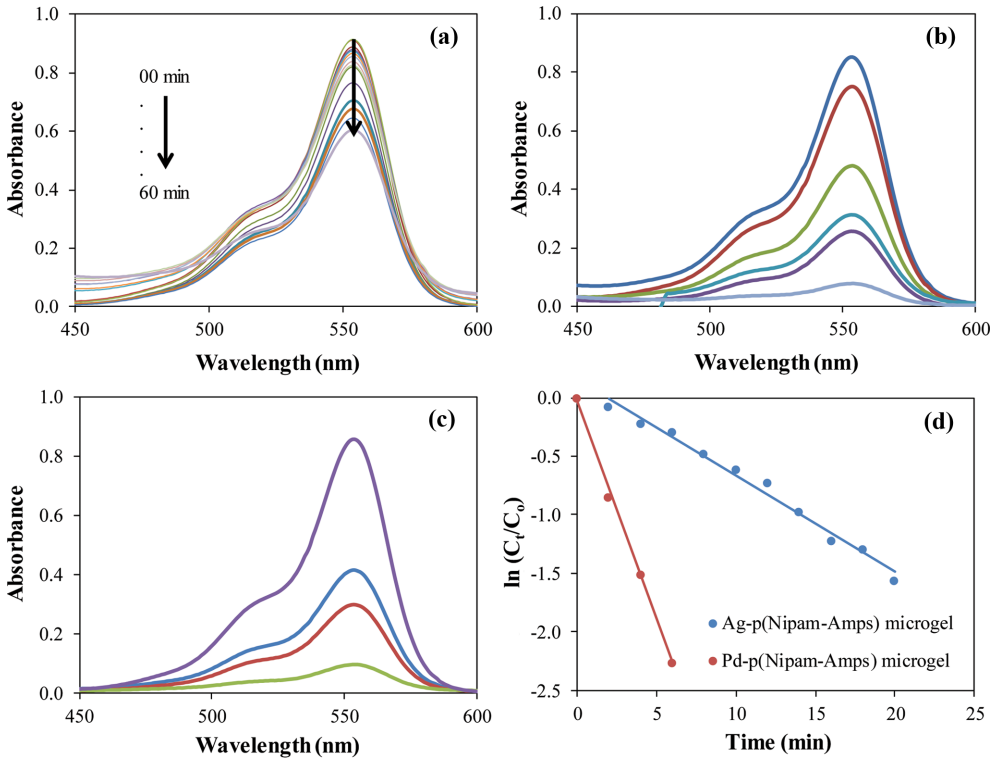


**Fig. 6. UV-Vis Absorption spectra for the reduction of Rhodamine B (a) in the presence of reducing agent but absence of catalyst (b) catalyzed by Ag-p(Nipam-Amps) (c) catalyzed by Pd-p(Nipam-Amps), (d) Pseudo first order plots for the catalytic reduction of Rhodamine B. Reaction conditions: Concentration and volume of Rhodamine B=0.016 mM, 20 ml, $NaBH_4$=0.02 g, Ag- or Pd-p(Nipam-Amps) microgel=20 μL, temperature=25 °C, pH=6.5.**

B dye was checked in the presence of $NaBH_4$ reducing agent. Initially, the reduction process was checked in the presence of only $NaBH_4$ and absence of catalyst. The reduction process was much too slow and only 43% decrease in the absorbance of specific sample was observed in 60 mins as depicted by UV-Vis spectra in Fig. 6(a). The probable reason for this is the high activation energy barrier associated with large potential difference between electron donors and acceptors. However, the addition of catalyst reduced the reaction time by lowering the activation energy barrier and increasing the rate of reaction. In the presence of Pd- and Ag-p(Nipam-Amps) hybrid microgel catalysts, more than 92% decrease in the absorbance of specific sample of rhodamine B was observed in just 12 and 6 mins, respectively, as depicted by UV-Vis spectra in Fig. 6(b) and 6(c). As $NaBH_4$ was utilized in the reaction in large excess, therefore it was assumed to be a pseudo-first-order reaction and rate of reaction was measured by using corresponding kinetic equation (Eq. (1)).

$$\ln(C_t/C_0) = -k_{app} \cdot t \quad (1)$$

where $C_t$ is the concentration at time (t), $C_o$ is the concentration at time=0 and $k_{app}$ is apparent rate constant. The graphical form of Eq. (1) is shown in Fig. 6(d). The values of $k_{app}$ were found from the slope of these plots. The apparent rate of reaction for the reduction of Rhodamin B catalyzed by Ag-p(Nipam-Amps) and Pd-p(Nipam-Amps) hybrid microgels was found to be 0.082 and 0.373 $min^{-1}$, respectively, under the same set of reaction conditions. It has been revealed from the EDX and TEM analysis that equivalent amounts of Ag-p(Nipam-Amps) and Pd-p(Nipam-Amps) hybrid microgels were having different content of Ag and Pd metals as well as the corresponding metal nanoparticles were also having different sizes, therefore surface area normalized rate constants ($k_{SA}$) were calculated for more precise comparison of the subject catalysts. Previously reported method [37,38] was used for the calculations of $k_{SA}$ and it was found 8.20 $Lmin^{-1}g^{-1}$ and 95.85 $Lmin^{-1}g^{-1}$ for Ag-p(Nipam-Amps) and Pd-p(Nipam-Amps) hybrid microgels, respectively. In the next experiments, we studied the effect of catalyst concentration on the reduction reaction. Three different amounts (20 μL, 40 μL, and 60 μL) of each of Ag-p(Nipam-Amps) and Pd-p(Nipam-Amps) were added in the reaction medium by keeping all other parameters exactly identical. The values $k_{app}$ were calculated by applying pseudo-first-order equation. With an increase in the catalyst dose from 20 to 60 μL the observed corresponding increase in $k_{app}$ was 0.082 to 0.571 $min^{-1}$, and 0.373 to 0.968 $min^{-1}$ in case of Ag-p(Nipam-Amps) microgel and Pd-p(Nipam-Amps) microgel, respectively. This rise in apparent reduction rate can be ascribed to the increasing number of active sites in catalyst, which increases the effective collision frequency and finally the catalytic reduction rate. Palladium-based catalyst catalytic activity is better from the literature value in which the degradation was completed in 60 mins for Rhodamine-B [39]. However, the corresponding change observed in $k_{SA}$ was 8.20 to 19.07 $Lmin^{-1}g^{-1}$ for Ag-p(Nipam-Amps) microgel catalyst and 95.85 to 83.08 $Lmin^{-1}g^{-1}$ for Pd-p(Nipam-Amps) microgel catalyst. In comparison with $k_{app}$, relatively smaller increase in $k_{SA}$ for Ag-p(Nipam-Amps) microgel cat-

alyst and a decrease in $k_{SA}$ for Pd-p(Nipam-Amps) microgel catalyst were observed. These observations can be attributed to the fact that the available catalytic sites per unit volume are increased from their optimum value for the reactants present in unit volume. By virtue of the fact of lower amount of reactant than the capacity of catalytic sites per unit volume, either a small increase or even a decrease in $k_{SA}$ in comparison to $k_{app}$ was observed.

**2. Effect of pH and Temperature on Catalyst Efficiency**

In this work, Ag and Pd nanoparticles were fabricated in p(Nipam-Amps) microgel networks. Among the components of microgel, Nipam is temperature responsive and Amps is pH responsive. The response of microgel system appears as swelling and shrinking of its network, which can affect the diffusion speed of reactants towards the surface of nanocatalysts and hence can affect the catalytic activity of the microgel-nanoparticle composites. Therefore, catalytic activity of the Ag- and Pd-p(Nipam-Amps) microgel catalysts was also studied at different pH values (2, 4, 6, 8, 10) and at different temperatures keeping the catalyst and $NaBH_4$ amount constant. Fig. 7(a) and 7(b) demonstrate the effect of pH and temperature on the surface area normalized rate constant for the catalytic reduction of rhodamine B, respectively. It is obvious that both the pH and temperature do not affect the nanoparticles Ag or Pd embedded in p(Nipam-Amps) microgel but have influence on the p(Nipam-Amps) microgel network. Therefore, effects of pH and temperature

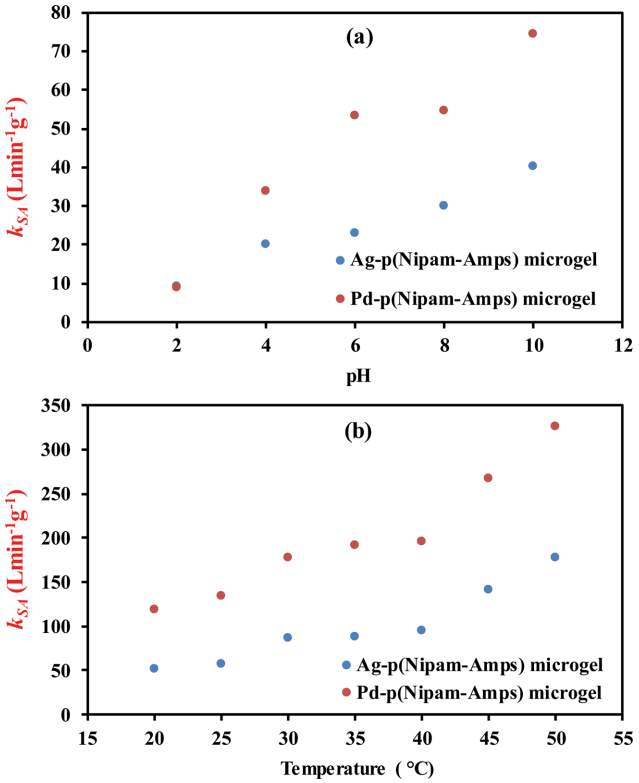


**Fig. 7. Plots of surface area normalized rate constant for the catalytic reduction of Rhodamine B as a function (a) pH and (b) temperature. Reaction conditions: Concentration and volume of Rhodamine B=0.016 mM, 20 ml, $NaBH_4$=0.01, Ag- or Pd-p(Nipam-Amps) microgel=20 μL, temperature=20-50 °C, pH=2-10.**

on reduction rate can be explained in terms swelling and shrinking in microgel network corresponding to variations in pH and temperature of the reaction medium.

It is clear from Fig. 7(a) that rate of degradation of Rhodamine B is low at low pH and increases by increasing the pH value. Actually at low pH, p(Nipam-Amps) microgel remains in shrunken state due to protonated sulfonic groups and hence hydrophobic character of the microgel network dominates. Under this situation, diffusion of reactant species into the microgel matrix to reach the surface of metal nanoparticles is hindered by closely packed polymer chains and diffusion rate becomes slow resulting in lower rate of reaction. With the increase in pH, catalytic activity was enhanced, which is mainly related to the production of negative charges on the sulfonic group that pull apart the polymer chains from each other. As the polymer chains are pulled apart, the hindrance against the diffusing reactants into the microgel matrix decreases and diffusion rate is increased, which in turn increases the rate of reaction. A study of the effect of temperature reveals that rate of reaction was low at low temperature and enhanced at higher temperature of the reaction medium, as depicted by Fig. 7(b). The increase in the rate of reaction is associated with the increase in average kinetic energy of the reactants because temperature of a medium is the average kinetic energy of the content of that medium. However, the increase in reaction rate slowed in the temperature range of 30-40 °C for both Ag- and Pd- p(Nipam-Amps) microgel catalysts. This can be attributed to shrinkage of microgel network accompanied by flow of water molecules in outward direction in this temperature region, which has been already shown in Fig. 2(b). So in the volume phase transition temperature region, first, an increase in the average kinetic energy and hence the diffusion ability of the reactants take place; second, the microgel network shrinks, resulting in increase in the resistance against the diffusion of reactants into the microgel network; finally, the water molecules absorbed in microgel network flow in the outward direction. The latter two actions dominate over the increased diffusion ability of reactants and as a result the rate of reaction is slowed down in this temperature window. Upon further increase in temperature above 40 °C, microgel network des not undergo any further shrinkage. Therefore, opposition against the diffusion is not increased but the diffusion ability of reactants is increased because of increase in average kinetic energy, and therefore the rate of reaction increases rapidly from 40 °C to 50 °C.

**3. Reduction of 4-Nitrophenol**

The color of the aqueous solution the 4-nitrophenol (4-NP) appears to be light yellow and its characteristic absorbance peak appears at 317 nm, as shown in Fig. 8(a). After the addition of $NaBH_4$, its color transformed to bright yellow due to the formation of phenolate ion with a red shift in absorption maximum to 400 nm, as shown in Fig. 8(a).

The catalytic conversion of P-nitrophenol (P-NP) into P-aminopehnol (P-AP) was also carried out as model reaction to test the catalytic performance of our prepared catalysts for the reduction of nitroaromatic compounds. The reaction is thermodynamically feasible, but it cannot proceed to complete degradation and remains dead slow without catalyst due to the large kinetic barrier between electron donors and acceptors of this reaction. Initially, the reduc-

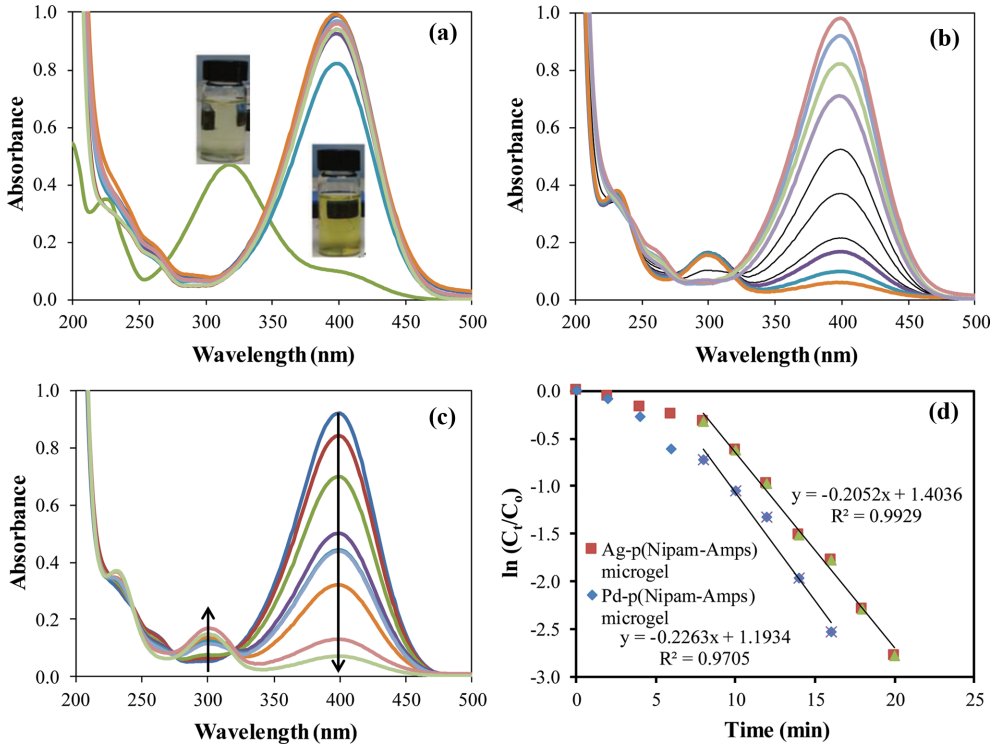


**Fig. 8. UV-Vis Absorption spectra of aqueous solution of P-Nitrophenol (a) in the absence and presence of reducing agent only (b) reduction catalyzed by Ag-p(Nipam-Amps) microgel (c) reduction catalyzed by Pd-p(Nipam-Amps) microgel (d) Pseudo first order plots for the catalytic reduction of P-Nitrophenol. Reaction conditions: Concentration and volume of P-nitrophenol=0.05 mM, 20 ml, $NaBH_4$= 0.01 g, Ag- or Pd-p(Nipam-Amps) microgel=20 μL, temperature=20-50 °C, pH=6.8.**

tion of P-NP was studied without catalyst; only in the presence of $NaBH_4$ and a very little decrease in the absorbance of P-NP was observed as shown in Fig. 8(a). Addition of a small amount of catalyst reduced the peak intensity at 400 nm quickly and another peak appeared at 300 nm associated to the formation of p-aminophenol whose intensity increased with the passage of time. By the end of the reaction, the bright yellow color of the solution changed to transparent, confirming the complete reduction of P-NP. The reduction of P-NP catalyzed by Ag-p(Nipam-Amps) microgel and Pd-p(Nipam-Amps) microgel catalysts was observed from UV Visible spctra shown in Fig. 8(b) and 8(c), respectively. The reaction follows the pseudo-first-order kinetics as the amount of $NaBH_4$ was taken in excess as compared to P-NP. The apparent rate constants for the reduction of P-NP catalyzed by Ag- and Pd-p(Nipam-Amps) microgel catalysts were calculated from the slopes of pseudo-first-order plots which are given in Fig. 8(d). The $k_{app}$ was found 0.205 and 0.226 $min^{-1}$ for Ag-p(Nipam-Amps) microgel and Pd-p(Nipam-Amps) microgel catalyst, respectively. The corresponding values of $k_{SA}$ were found to be 20.5 and 58.2 $Lmin^{-1}g^{-1}$ for Ag-p(Nipam-Amps) microgel and Pd-p(Nipam-Amps) microgel catalyst, respectively, representing that Pd-p(Nipam-Amps) microgel was having much greater catalytic efficiency as compared to Ag-p(Nipam-Amps) microgel catalyst.

## CONCLUSIONS

P(Nipam-Amps) microgels were prepared and fabricated with Ag and Pd NPs. The p(Nipam-Amps) microgel exhibited volume phase transition around a temperature of 35 °C and pH of 8. The p(Nipam-Amps) microgel has served as potential stabilizing agent and reactor for the formation of Ag and Pd NPs as demonstrated by TEM images without noticeable aggregates. The size of Pd NPs was smaller as compared to that of Ag NPs. The XRD analysis affirmed that p(Nipam-Amps) microgel was amorphous while Ag- and Pd-p(Nipam-Amps) microgel was attributed crystalline nature. Thermal studies showed that the prepared catalysts were thermally stable below 300 °C, so could be effectively applied below this temperature for catalytic role. P(Nipam-Amps) microgel containing both the Ag and Pd NPs showed potential to catalyze the reduction of dyes and nitrophenols. The catalytic activity was succefully controlled by temperature and pH of the reaction medium. Pd-p(Nipam-Amps) microgel showed better catalytic activity than Ag-p(Nipam-Amps) microgel.

## ACKNOWLEDGEMENTS

The authors are grateful for the financial support provided by the National Natural Science Foundation of China Projects (20934005 and 21274136) and the Fundamental Research Funds for the Central Universities. One of the authors, Mr. Abdul Haleem, wishes to acknowledge Chinese Scholarship Council (CSC) for granting him a scholarship for his Ph.D studies. M. Siddiq wishes to acknowledge Chinese Academy of Sciences for a three month fellowship as a visiting scholar to work in the USTC.

## REFERENCES


1. M. A. Hassaan and A. El Nemr, *Am. J. Environ. Sci. Eng.*, **1**, 64 (2017).
2. A. J. Whelton, L. McMillan, M. Connell, K. M. Kelley, J. P. Gill, K. D. White, R. Gupta, R. Dey and C. Novy, *Environ. Sci. Technol.*, **49**, 813 (2015).
3. M. S. Hernadez, M. P. Tenango and R. G. Mateos Eds., Intech Open, London (2017).
4. P. Kovacic and R. Somanathan, *J. Appl. Toxicol.*, **34**, 810 (2014).
5. I. Ali, M. Asim and T. A. Khan, *J. Environ. Manage.*, **113**, 170 (2012).
6. V. K. Gupta, I. Ali, T. A. Saleh, A. Nayak and S. Agarwal, *RSC Adv.*, **2**, 6380 (2012).
7. J. Kim, K. Kim, H. Ye, E. Lee, C. Shin, P. L. McCarty and J. Bae, *Environ. Sci. Technol.*, **45**, 576 (2010).
8. A. S. Crampton, M. D. Rötzer, C. J. Ridge, F. F. Schweinberger, U. Heiz, B. Yoon and U. Landman, *Nat. Commun.*, **7**, 10389 (2016).
9. Y. Lu, J. Wang, L. Yu, L. Kovarik, X. Zhang, A. S. Hoffman, A. Gallo, S. R. Bare, D. Sokaras and T. Kroll, *Nat. Catal.*, **2**, 149 (2019).
10. C.-T. Kuo, Y. Lu, L. Kovarik, M. H. Engelhard and A. M. Karim, *ACS Catal.*, **9**, 11030 (2019).
11. Z. H. Farooqi, S. R. Khan and R. Begum, *Mater. Sci. Technol.*, **33**, 129 (2017).
12. R. Begum, K. Naseem and Z. H. Farooqi, *J. Sol-Gel Sci. Technol.*, **77**, 497 (2016).
13. F. Naseer, M. Ajmal, F. Bibi, Z. H. Farooqi and M. Siddiq, *Polym. Compos.*, **39**, 3187 (2018).
14. F. Bibi, M. Ajmal, F. Naseer, Z. Farooqi and M. Siddiq, *Int. J. Environ. Sci. Technol.*, **15**, 863 (2018).
15. V. A. Ganesh, A. Baji and S. Ramakrishna, *RSC Adv.*, **4**, 53352 (2014).
16. R. Contreras-Cáceres, A. Sánchez-Iglesias, M. Karg, I. Pastoriza-Santos, J. Pérez-Juste, J. Pacifico, T. Hellweg, A. Fernández-Barbero and L. M. Liz-Marzán, *Adv. Mater.*, **20**, 1666 (2008).
17. J. Liu, T. Shu, L. Su, X. Zhang and M. J. Serpe, *RSC Adv.*, **8**, 16850 (2018).
18. Z. H. Farooqi, S. R. Khan, R. Begum and A. Ijaz, *Rev. Chem. Eng.*, **32**, 49 (2016).
19. R. Begum, Z. H. Farooqi and S. R. Khan, *Int. J. Polymer. Mater. Polymer. Biomater.*, **65**, 841 (2016).
20. Z. H. Farooqi, S. R. Khan, T. Hussain, R. Begum, K. Ejaz, S. Majeed, M. Ajmal, F. Kanwal and M. Siddiq, *Korean J. Chem. Eng.*, **31**, 1674 (2014).
21. Z. H. Farooqi, A. Ijaz, R. Begum, K. Naseem, M. Usman, M. Ajmal and U. Saeed, *Polym. Compos.*, **39**, 645 (2018).
22. D.-M. Han, Q. M. Zhang and M. J. Serpe, *Nanoscale*, **7**, 2784 (2015).
23. Y.-Y. Liu, X.-Y. Liu, J.-M. Yang, D.-L. Lin, X. Chen and L.-S. Zha, *Colloids Surf., A*, **393**, 105 (2012).
24. N. Sahiner, S. Butun and T. Turhan, *Chem. Eng. Sci.*, **82**, 114 (2012).
25. L. A. Shah, J. Ambreen, I. Bibi, M. Sayed and M. Siddiq, *J. Chem. Soc. Pak.*, **38**, 850 (2016).
26. Q. M. Zhang, W. Wang, Y.-Q. Su, E. J. M. Hensen and M. J. Serpe, *Chem. Mater.*, **28**, 259 (2016).
27. M. Ajmal, Z. H. Farooqi and M. Siddiq, *Korean J. Chem. Eng.*, **30**, 2030 (2013).
28. E. Larsson, A. Boujemaoui, E. Malmstrom and A. Carlmark, *RSC Adv.*, **5**, 77643 (2015).
29. A. Vakifli, G. B. Demirel and T. Caykara, *J. Appl. Polym. Sci.*, **117**, 817 (2010).
30. C. Zhang and A. J. Easteal, *J. Appl. Polym. Sci.*, **104**, 1723 (2007).
31. K. Varaprasad, S. Ravindra, N. N. Reddy, K. Vimala and K. M. Raju, *J. Appl. Polym. Sci.*, **116**, 3593 (2010).
32. K. Mallikarjuna, C. Bathula, G. D. Reddy, N. K. Shrestha, H. Kim and Y. Y. Noh, *Int. J. Biol. Macromol.*, **126**, 352 (2019).
33. A. M. Atta, A. K. Gafer, H. A. Al-Lohedan, M. Abdullah, A. M. Tawfeek and A. O. Ezzat, *Molecules*, **24**, 3867 (2019).
34. N. Ali, G. Bi, A. Khesro, M. Khan, J. Lang, A. Samreen and H. Wu, *New J. Chem.*, **42**, 18991 (2018).
35. R. Y. Zhao, X. X. Sun, Y. R. Jin, J. S. Han, L. Wang and F. S. Liu, *J. Mater. Sci.*, **54**, 5445 (2019).
36. Y. M. Zhang, X. Y. Quek, L. L. Wu, Y. J. Guan and E. J. Hensen, *J. Mol. Catal. A-Chem.*, **379**, 53 (2013).
37. F. He and D. Zhao, *Environ. Sci. Technol.*, **39**, 3314 (2005).
38. R. Singh, V. Misra, M. K. R. Mudiam, L. K. S. Chauhan and R. P. Singh, *J. Hazard. Mater.*, **237**, 355 (2012).
39. C. M. Magdalane, K. Kaviyarasu, J. J. Vijaya, B. Siddhardha, B. Jeyaraj, J. Kennedy and M. Maaza, *J. Alloy Compd.*, **727**, 1324 (2017).